Gain–Phase Characteristics of Groundwater Responses to Barometric Pressure: Interpreting Subsurface Confinement in Layered Systems

Zixuan Qin[1], Jian Guo[1†], Peter J. Cleall[2] , Qiang Xu[1], John A. Cherry[3], and Beth L. Parker[3]

[1]State Key Laboratory of Geo-hazard Prevention and Geo-environment Protection, Chengdu University of Technology, Chengdu 610059, China.

[2] Cardiff University School of Engineering, Cardiff University, Cardiff CF243AA, Wales.

[3]Morwick G360 Groundwater Research Institute, College of Engineering & Physical Sciences, University of Guelph, Guelph N1G2W1, Canada.

Corresponding author: Jian Guo (guojian2014@cdut.edu.cn)

†State Key Laboratory of Geo-hazard Prevention and Geo-environment Protection, Chengdu University of Technology, Chengdu 610059, China. Tel: +86 1398 171 1984. ORCID ID: 0000-0003-0359-8354

Keywords:

Barometric response; Aquifer confinement; Frequency analysis; Layered systems; Groundwater

Highlights:

- Time- and frequency-domain analyses reveal lithology-controlled barometric responses in layered systems
- Gain–phase relationships differ systematically between unconfined and confined-like response regimes
- Gain–phase co-variation trends provide insight into confinement-related pressure transmission behavior

Abstract

Aquifer confinement plays a key role in controlling vertical hydraulic connectivity and pressure transmission, yet its identification in heterogeneous systems remains challenging using conventional methods. This study applies frequency-domain barometric response functions (BRF) to analyze groundwater response to atmospheric pressure. A six-port Continuous Multichannel Tubing (CMT) system was installed in a layered aquifer. Long-term groundwater, barometric pressure, and precipitation data were analyzed using cross-correlation, FFT, and BRF methods. Time- and frequency-domain analyses reveal pronounced lithology-controlled differences. Ports screened in sandstone units exhibited stronger barometric signals and shorter response lags, while mudstone-adjacent ports showed attenuated responses. Detailed BRF analysis was performed on two representative ports: Port 1 (upper sandstone above mudstone) and Port 6 (lower sandstone below mudstone). The upper sandstone showed a negative gain-phase co-variation, characteristic of unconfined systems, while the lower sandstone exhibited a positive gain-phase relationship, suggesting functional confinement. These findings highlight the utility of BRF analysis for interpreting pressure transmission and confinement in vertically heterogeneous aquifers.

1 Introduction

Aquifers often exhibit vertical heterogeneity, and variations in confinement-related hydraulic behavior can substantially influence surface–groundwater interactions (Gulley et al., 2013), solute transport (Koh et al., 2016; Wang et al., 2024), waste storage (Maliva & Walker, 1998; Liu et al., 2025), and groundwater resource management (Bui et al., 2012; Rausch & Dirks, 2024). Conventional approaches for characterizing aquifer confinement, such as pumping tests and borehole drilling, are often constrained by subjectivity, high costs, disturbance, and limited capacity for continuous monitoring. Periodic barometric tides (e.g., diurnal and semi-diurnal tides) induce groundwater level fluctuations, offering a natural perturbation means to infer aquifer hydraulic properties (Merritt, 2004; Acworth et al., 2017; McMillan et al., 2019; Qi et al., 2023). Thus, analyzing groundwater responses to barometric pressure fluctuations can provide valuable insights into aquifer confinement and vertical hydraulic connectivity.

Groundwater level responses to atmospheric loading are governed by multiple factors, including well construction, aquifer hydraulic properties, and site-specific geological conditions, resulting in a wide range of barometric response behaviors. These responses are commonly discussed in

terms of confined, semi-confined, and unconfined conceptual end-members, reflecting contrasting pressure transmission pathways and storage mechanisms (Rojstaczer & Agnew, 1989). In confined systems, barometric pressure variations are generally transmitted rapidly to the pore fluid and shared between the aquifer matrix and groundwater. Under ideal conditions where wellbore storage and skin effects are negligible, the resulting groundwater level fluctuations can be approximated by a constant response, referred to as the static barometric efficiency (Jacob, 1940). By contrast, in unconfined and semi-confined systems, thick unsaturated zones or low-permeability confining layers may attenuate and delay pressure transmission, leading to reduced and time-dependent groundwater level responses (Weeks, 1979; Spane, 2002; Lai et al., 2013). Such delayed propagation can generate transient pressure gradients between the aquifer and the well, causing groundwater responses that vary across both time- and frequency-domains. Barometric response functions (BRF) provide a quantitative framework for characterizing these response behaviors and for examining the physical mechanisms governing pressure transmission and damping.

Rasmussen and Crawford (1997) introduced a regression–deconvolution approach to derive time-domain BRFs, characterizing the shape and lag of groundwater level responses to atmospheric pressure fluctuations. Subsequent studies have applied to estimate barometric efficiency (BE), identify wellbore effects, and assess aquifer confinement (Landmeyer, 1996; Butler et al., 2011; Patton et al., 2021; Akara et al., 2025). However, time-domain interpretations are often sensitive to uncertainties in unsaturated zone thickness, leakage conditions, and nonstationary forcing, and response lag is difficult to quantify robustly under high-frequency perturbations. Frequency-domain BRF provide a more time-invariant and mathematically rigorous framework, wherein the gain and phase functions characterize aquifer responses to

77 periodic loading and reveal differences in transmission mechanisms across temporal scales. In
78 frequency-domain BRF analyses, aquifer responses to barometric loading are commonly
79 characterized using gain and phase functions. Gain describes the ratio of groundwater level
80 fluctuation amplitude to atmospheric pressure forcing at a given frequency, reflecting the
81 efficiency of pressure transmission into the subsurface. Phase represents the temporal offset
82 between the two signals in the frequency-domain and provides information on the characteristic
83 response time and damping behavior of the aquifer system (Rojstaczer, 1988; Evans et al., 1991).
84 From a system-response perspective, gain and phase are complementary descriptors of the same
85 physical process and are inherently linked across frequencies. Analytical solutions have been
86 developed for semi-confined aquifers by Rojstaczer (1988) and Evans et al. (1991), and for
87 unconfined conditions by Rojstaczer and Riley (1990) and Quilty and Roeloffs (1991).
88 Frequency-domain BRF have been widely used to examine spatial variability in barometric
89 responses across wells (Oldling et al., 2015; Sun & Xiang, 2020; Kennel & Parker, 2024) and to
90 monitor changes in aquifer properties following events such as earthquakes, pumping, and
91 landslides (Elkhoury et al., 2006; Hessein et al., 2013; Sun & Xiang, 2019; Zhang et al., 2019;
92 Thomas et al., 2023; Qi et al., 2024; Qin et al., 2025). However, systematic evaluation of gain–
93 phase behavior across vertically distributed monitoring depths remains limited, particularly with
94 respect to interpreting confinement-related response behavior in layered aquifer systems.

95 In this study, we aim to evaluate whether frequency-domain gain–phase relationships can be
96 used as a diagnostic indicator of aquifer confinement and vertical hydraulic connectivity in
97 layered groundwater systems. To this end, a Continuous Multichannel Tubing (CMT) monitoring
98 system was deployed to obtain long-term, vertically resolved groundwater level records under
99 natural atmospheric forcing. By focusing on the systematic behavior of gain and phase across

monitoring depths, rather than on individual response metrics alone, this study seeks to address a key limitation of existing BRF applications in heterogeneous aquifers. The proposed framework emphasizes the interpretive value of gain–phase co-variation and provides a physically grounded approach for assessing confinement-related hydraulic behavior in multilevel monitoring wells.

It should be noted that confinement in this study is operationally defined in the context of its functional impact on pressure transmission, as inferred from observed barometric response behavior, rather than as a strict stratigraphic classification. Unlike traditional rigid-flow theory, which treats confinement as a static condition governed by impermeable layers, the observed responses in this study are more consistent with a poroelastic framework, in which pressure transmission is controlled by the elastic and diffusive properties of the aquifer system and overlying materials. Accordingly, confinement is interpreted through frequency-dependent gain–phase characteristics, which reflect the effective vertical hydraulic connectivity and pressure transmission behavior under atmospheric loading.

2 Study Area and Data

2.1 Study Area and Monitoring Network

The Kualiangzi monitoring well is located in Sichuan Province, southwestern China (30°39′01″N, 104°53′40″E), situated on the midslope of a local hillslope groundwater system (Figure 1a, b). The study area is predominantly covered by a layer of residuals and diluvials (Q_4), consisting of silty clay mixed with a small amount of gravel. The underlying bedrock comprises interbedded sandstone and mudstone of the Upper Penglaizhen Group of the Jurassic Period (J_3p) (Figure 1d).

The well–aquifer system and borehole completion details are illustrated in Figure 1c. The monitoring well is completed as a sealed, multi-level system using Continuous Multichannel

Tubing (CMT), which enables depth-discrete groundwater level monitoring while minimizing hydraulic interference between stratigraphic units. The borehole diameter is 100 mm, and the CMT tubing has an outer diameter of 43 mm. Six monitoring ports (Ports 1–6) are installed at depths corresponding to the center of the sand-packed intervals: 21.9–22.9 m, 24.0–24.3 m, 26.4–26.7 m, 28.0–28.3 m, 30.9–31.2 m, and 34.3–35.3 m, respectively. Continuous core data from the well site revealed a stratigraphic sequence of approximately 6 m of gravelly soil, 20 m of sandstone, 6 m of mudstone, and 5.5 m of sandstone. The thickness of the unsaturated zone is approximately 20 m.

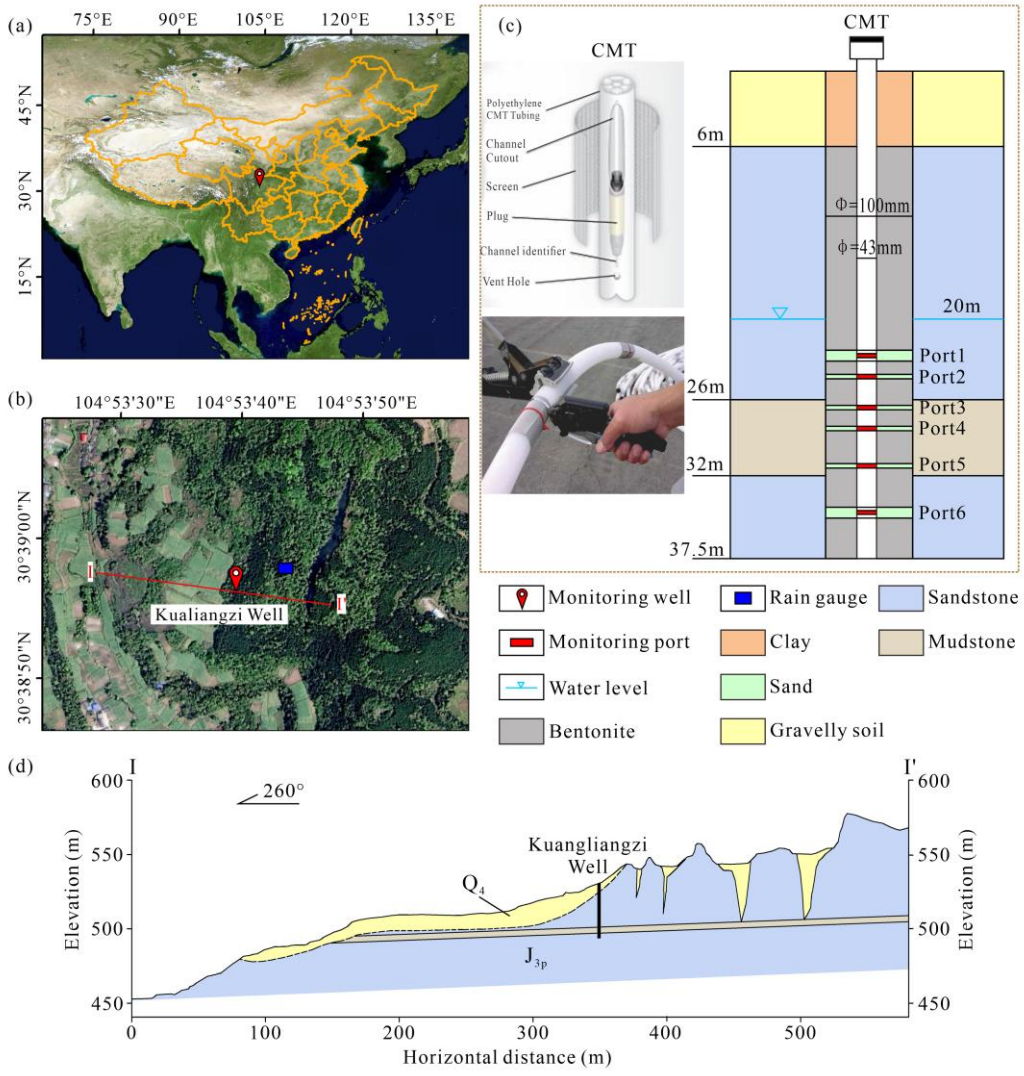

Figure 1. (a) The location map of the Kualiangzi well, (b) Topography in the Kualiangzi area around the Kualiangzi well (red dot), (c) Schematic diagram of the CMT well illustrating port depths and borehole construction, and (d) Simplified geological profile and the monitoring well location of section I-I′.

2.2 Data Collection and Observation

Groundwater levels at each monitoring port were measured using Micron MP102 gauge piezometers, each with a measurement resolution of 0.01 m and a sampling interval of 10 min. Barometric pressure was recorded using a Baro-Diver with a precision of 0.01 mH_2O (0.1 hPa) and sampling interval of 10 min. Rainfall data were obtained from a real-time precipitation monitoring station located within the study area, with a temporal resolution of 1 hour and an accuracy of 0.01 mm. It is important to note that sensor resolution plays a critical role in the observed data. The limits of analogue-to-digital conversion are reflected in the data, and any signals smaller than this threshold are not captured by the sensors.

As observed in Fig. 2, groundwater levels in Ports 1 and 2 show a clear response to rainfall events, while the relatively elevated heads at Ports 5 and 6 suggest a contrasting hydraulic behavior compared to the shallow monitoring ports. Across all six monitored depths, groundwater levels generally declined in response to rising barometric pressure and rose when atmospheric pressure decreased. Peaks in barometric pressure commonly coincided with troughs in groundwater levels, indicating a predominantly negative correlation (Wang & Manga, 2023).

Although barometric responses appeared broadly synchronous across depths within the borehole, a measurable lag time was observed between atmospheric pressure changes and groundwater level responses. Such temporal delays are consistent with previous observations (Furbish, 1991;

Rasmussen & Crawford, 1997; Valois et al., 2023) and reflect site-specific hydraulic and well-aquifer interaction processes.

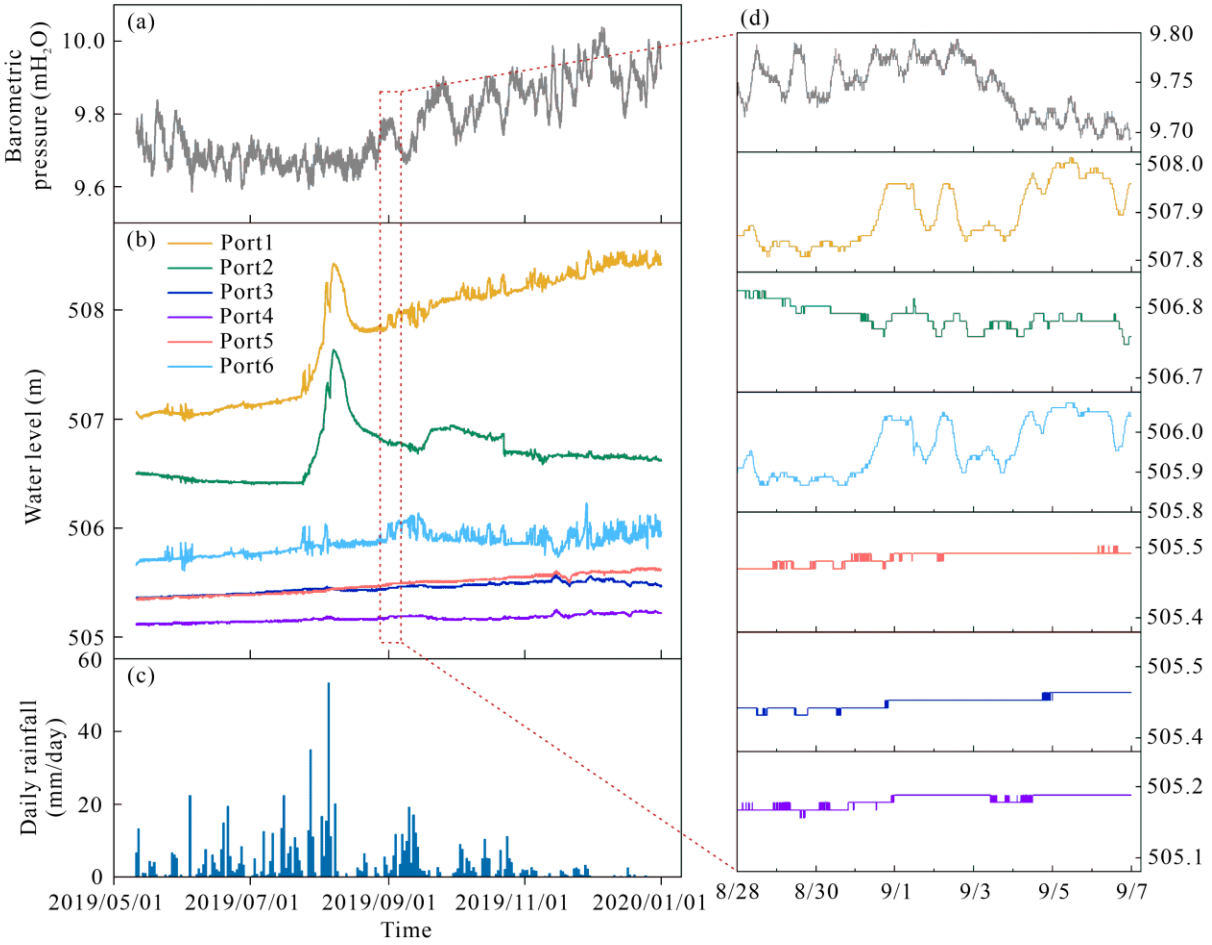

Figure 2. Time series data from 10 May to 31 December 2019, including: (a) barometric pressure; (b) groundwater levels at six monitoring ports; (c) rainfall; and (d) an enlarged view of groundwater levels from 28 August to 7 September 2019.

3 Methods and Results

3.1 Data Preprocessing

Data preprocessing is essential for isolating groundwater responses to barometric pressure, as groundwater level fluctuations are influenced by multiple hydrological factors (Jan et al., 2007).

In the study area, rainfall represents the dominant non-barometric forcing and must be removed prior to barometric response analysis. Although the region experiences substantial precipitation, the presence of a thick unsaturated zone in the central part of the slope body can attenuate and delay the transmission of recharge signals to groundwater (Xu et al., 2015).

High-pass Butterworth filtering was applied to groundwater level time series to suppress low-frequency components associated with rainfall recharge and long-term trends, while preserving barometric pressure–induced fluctuations. A first-order Butterworth filter was implemented using a forward–backward (zero-phase) filtering scheme (filtfilt function in MATLAB), ensuring that no phase distortion was introduced during preprocessing. Figure 3 compares the original and filtered groundwater level time series. Due to pronounced differences in rainfall sensitivity across monitoring depths and time periods, cutoff frequencies were selected adaptively to effectively remove recharge-related signals. For Ports 1 and 2, which exhibited strong rainfall-induced groundwater level rises during periods of intense precipitation (21 July–15 August 2019), a higher cutoff frequency of 0.1 cycles per day was applied. For other periods at these ports (11 May–20 July and 16 August–31 December 2019) and Ports 3 to 6 to ensure consistency across monitoring ports, a uniform cutoff frequency of 0.02 cpd was applied to all monitoring depths. As shown in Fig. 3, this filtering strategy effectively removed recharge-related fluctuations, enabling subsequent analyses to focus on groundwater responses to atmospheric pressure variations. To evaluate the robustness of the BRF results to the choice of cutoff frequency, a sensitivity analysis using alternative filtering parameters was conducted, and the results are presented in Supplementary Material S1.

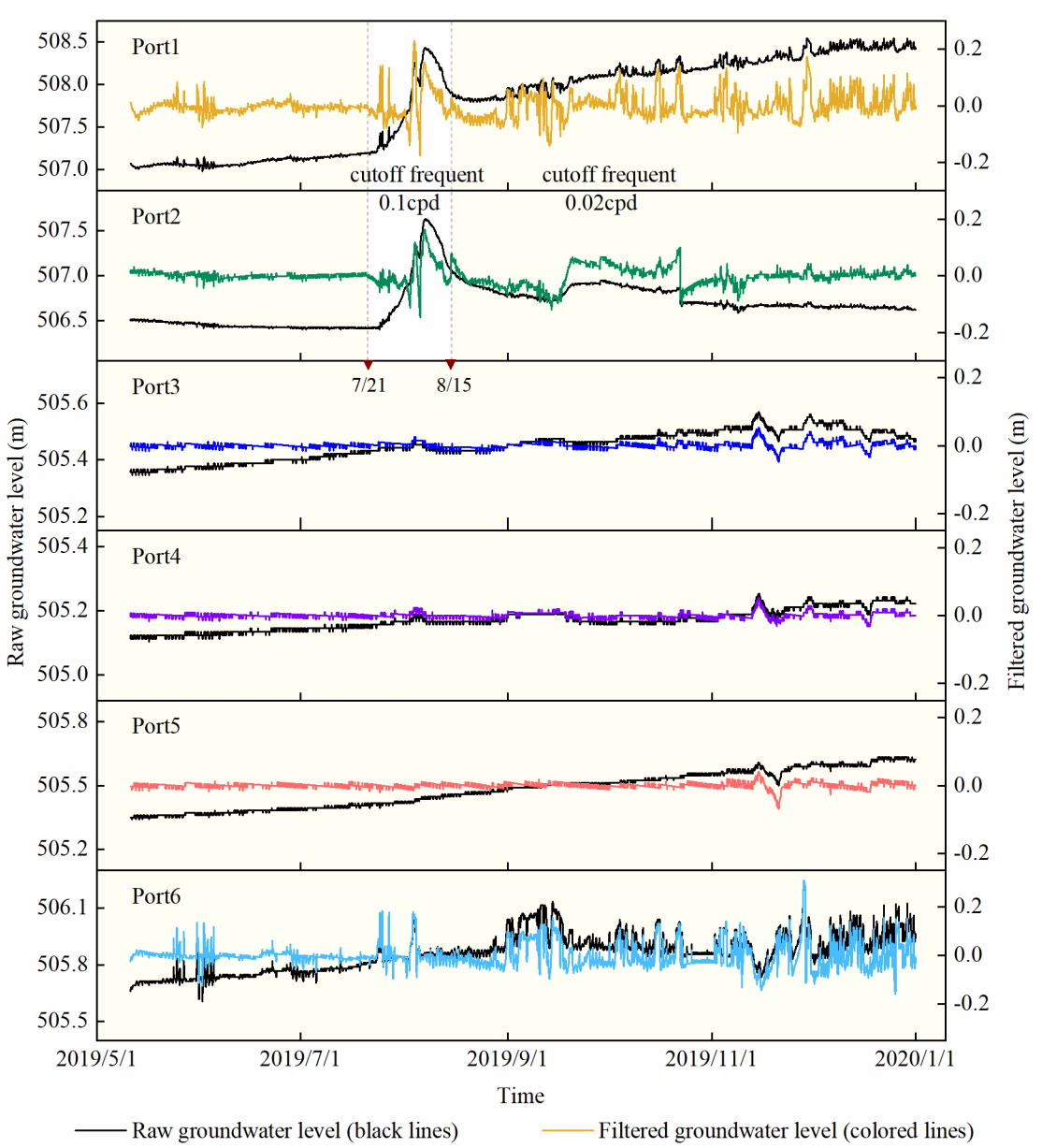

Figure 3. Groundwater level time series at Ports 1–6, showing raw water level signals (black lines) and filtered signals with recharge effects removed (colored lines).

3.2 Cross-Correlation Analysis

The cross-correlation function (CCF) is a statistical tool commonly used to quantify the relationship between an input time series $\{x_t\}_{t=1}^{n}$ and an output time series $\{y_t\}_{t=1}^{n}$ by evaluating their correlation at different time lags (Padilla & Pulido-Bosch, 1995; Molénat, 1999; Shi, 2018).

In groundwater studies, CCF analysis is widely applied to identify the delayed responses of groundwater levels to external forcings, such as atmospheric pressure. The magnitude of the cross-correlation coefficient reflects the strength of the relationship between the two series, while the lag at which the correlation reaches an extremum provides an estimate of the response delay (Manna, 2022). In this study, the cross-correlation function between barometric pressure and groundwater level is defined as:

$$CCF_{BP,GW}(\tau) = \frac{cov[BP(t),GW(t+\tau)]}{\sigma BP \sigma GW} \quad (1)$$

where $BP(t)$ and $GW(t)$ denote barometric pressure and groundwater level at time t, respectively, σ_{BP} and σ_{GW} are their standard deviations, and τ is the time lag. Positive values of τ indicate a delayed groundwater response to barometric pressure variations.

CCF analysis requires quasi-stationary signals. Applying CCF to the entire filtered dataset, which may still contain nonstationary components related to recharge and long-term trends, could bias the lag time estimation. Therefore, CCF was performed on short, stationary windows dominated by barometric forcing. Groundwater level data, originally recorded at 10-minute intervals, were downsampled to hourly intervals prior to cross-correlation analysis to reduce high-frequency noise and enhance the stability of lag estimations. This resampling does not affect the frequency band of interest and preserves all relevant barometric signals.

Both barometric pressure and groundwater level time series were high-pass filtered with a cutoff frequency of 0.02 cpd to remove low-frequency components related to recharge and long-term trends. This filtering was essential to isolate short-term pressure-driven signals and ensure stable lag time estimation. As shown in Figure 4, to assess the temporal stability of the barometric response and minimize the influence of nonstationary signals, cross-correlation analysis was

performed on three representative 24-hour time windows selected from early, middle, and late stages of the monitoring period (mid-May, early September, and late December 2019, respectively). These 24-hour windows were objectively selected based on (i) minimal rainfall, (ii) stable groundwater levels, and (iii) high barometric coherence, ensuring that the analyzed signals primarily reflected pressure-driven groundwater responses. Each window also captured at least one full diurnal barometric cycle while minimizing the influence of nonstationary recharge signals. For each window, CCF was computed between atmospheric pressure and groundwater level time series, with the response lag times identified based on the lag corresponding to the maximum negative correlation within the physically meaningful positive-lag range.

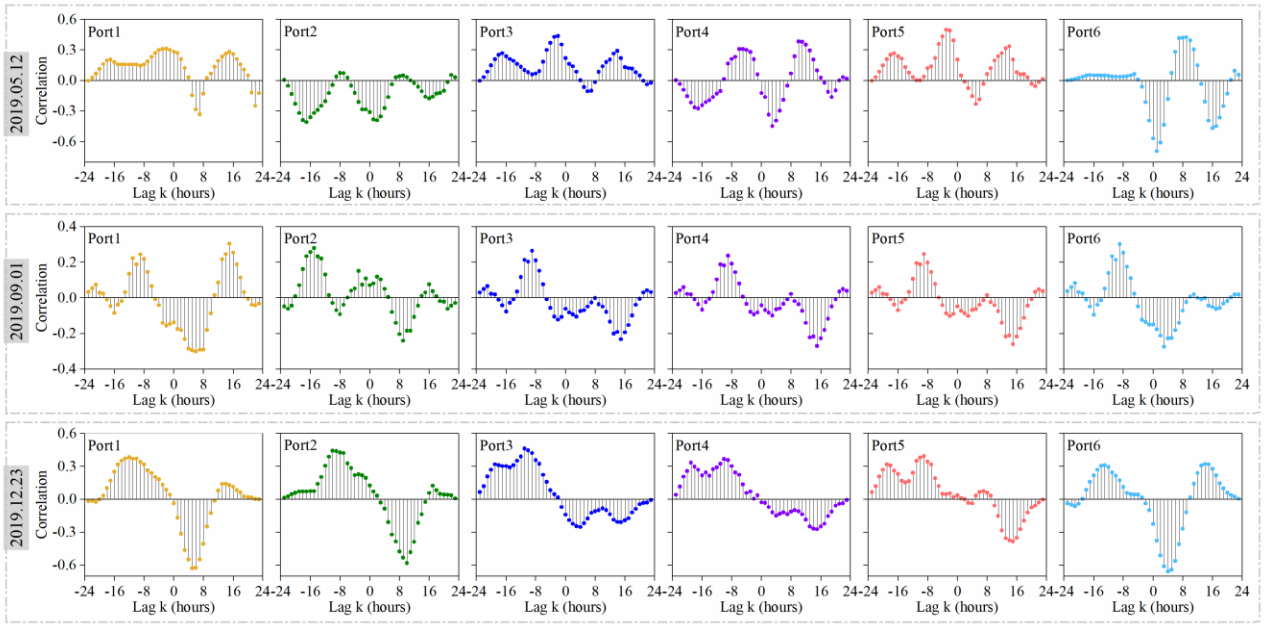

Figure 4. Cross-correlation functions between barometric pressure and groundwater levels at Ports 1–6, evaluated over three representative 24-h periods. The peak negative correlation identifies the lag time of groundwater response to barometric loading.

Across all three analysis windows, groundwater levels at all monitoring ports generally exhibited a negative correlation with atmospheric pressure at positive lag times, indicating a consistent

inverse barometric response. Temporally, during the early stage of the monitoring period, the lag corresponding to the strongest negative correlation ranged from approximately 1 to 7 hours across Ports 1–6. In the middle stage, the lag times increased to about 3–15 hours, and a comparable range was observed during the late stage of the monitoring period.

From a vertical perspective, monitoring ports located within or immediately adjacent to the low-permeability mudstone layer (Ports 1–5) consistently exhibited longer lag times than those situated in sandstone units. The lower sandstone aquifer (Port 6) responded most rapidly to atmospheric pressure fluctuations, while the upper sandstone aquifer (Port 1) displayed intermediate lag characteristics. These differences reflect the contrasting pressure transmission mechanisms associated with lithological heterogeneity. Atmospheric pressure variations can be transmitted relatively rapidly to the lower sandstone aquifer at Port 6 through elastic deformation of the aquifer framework, resulting in shorter response lags. In contrast, Ports 2–5, located within or strongly influenced by the mudstone layer, exhibited substantially delayed responses, indicating pronounced attenuation and retardation of pressure propagation in low-permeability media. The intermediate lag behavior observed at Port 1 may suggest the influence of unsaturated zone thickness on the barometric response. Although the absolute lag times varied among different time windows, the relative depth-dependent pattern of barometric response remained stable, indicating that the time-domain groundwater response to atmospheric loading derived from cross-correlation analysis is temporally robust.

3.3 Fast Fourier Transform

High-frequency groundwater monitoring data commonly contain multiple overlapping signals that are difficult to interpret directly in the time domain. To extract dominant periodic components and clarify the underlying spectral structure, frequency-domain analysis based on

253 the Fast Fourier Transform (FFT) is widely applied (Welch, 1967; Davis, 1986). The FFT
254 transforms a time series from the time domain into the frequency domain, decomposing periodic
255 signals into sinusoidal components with distinct frequencies and amplitudes. In hydrogeological
256 contexts, this approach facilitates the recognition of cyclic responses associated with external
257 forcing and aquifer system behavior (Barco, 2010).

258 FFT analysis was performed on both atmospheric pressure and groundwater level time series
259 using 10-min evenly sampled data. Groundwater level records were analyzed after high-pass
260 filtering to suppress low-frequency recharge-related variations and long-term trends, whereas
261 atmospheric pressure data were analyzed in their original form. For a discretely sampled
262 groundwater level time series $x(n)$ with a constant sampling interval Δt, the discrete Fourier
263 transform (DFT) is expressed as:

264 $$\mathrm{X}(k) = \sum_{n=0}^{N-1} x(n) e^{-j2\pi k \mathrm{n}/N}, \quad \mathrm{k}=0,1, \ldots, \mathrm{N}\text{-}1 \qquad (2)$$

265 where N is the total number of samples, $X(k)$ represents the complex Fourier coefficient at the
266 k-th frequency component, and j is the imaginary unit.
267 Figure 5 and Table 1 present the FFT spectra of atmospheric pressure and groundwater levels,
268 together with the amplitudes of the main spectral components. The results show that the
269 amplitudes of the solid Earth tide components, including O_1 (Lunar diurnal tide) and M_2 (Lunar
270 semi-diurnal tide), are consistently small in the groundwater level spectra (generally < 1 mm).
271 This indicates that solid Earth tides contribute negligibly to the observed groundwater level
272 fluctuations at the study site (Weeks, 1979; Acworth et al., 2017). The barometric pressure
273 spectrum is dominated by broadband energy below approximately 0.8 cpd, superimposed with
274 distinct spectral peaks at 1 cpd and 2 cpd. These peaks correspond to the diurnal (S_1) and

semidiurnal (S_2) atmospheric tides, which are primarily driven by thermal forcing associated with solar heating and ozone absorption (Chapman and Lindzen, 1969). After high-pass filtering, the groundwater level spectra at all six monitoring ports exhibit corresponding peaks at 1 cpd and 2 cpd, indicating persistent groundwater responses to atmospheric tidal loading throughout the monitoring period.

Notably, marked depth-dependent differences in spectral amplitudes are observed. Monitoring ports located above the mudstone layer (Port 1) and below it (Port 6) exhibit strong and well-defined S_1 and S_2 peaks, with amplitudes substantially higher than those recorded at ports situated within or adjacent to the mudstone layer (Ports 2–5). For example, the S_1 and S_2 amplitudes at Port 1 reach 12.39 mm and 3.66 mm, respectively, while Port 6 exhibits even larger amplitudes of 13.64 mm (S_1) and 6.73 mm (S_2). In contrast, the corresponding amplitudes at Ports 2–5 generally remain within 1–2 mm and, in some cases, approach the background noise level.

This pronounced vertical contrast highlights the controlling role of lithological structure on the transmission of atmospheric pressure signals. The mudstone layer, characterized by low permeability and strong damping capacity, significantly attenuates vertical pressure propagation, resulting in muted barometric responses within and near the layer. In contrast, the sandstone aquifers located above and below the mudstone allow more efficient transmission of atmospheric loading through elastic deformation or hydraulic adjustment mechanisms, producing clearer and stronger atmospheric tide signatures in groundwater levels.

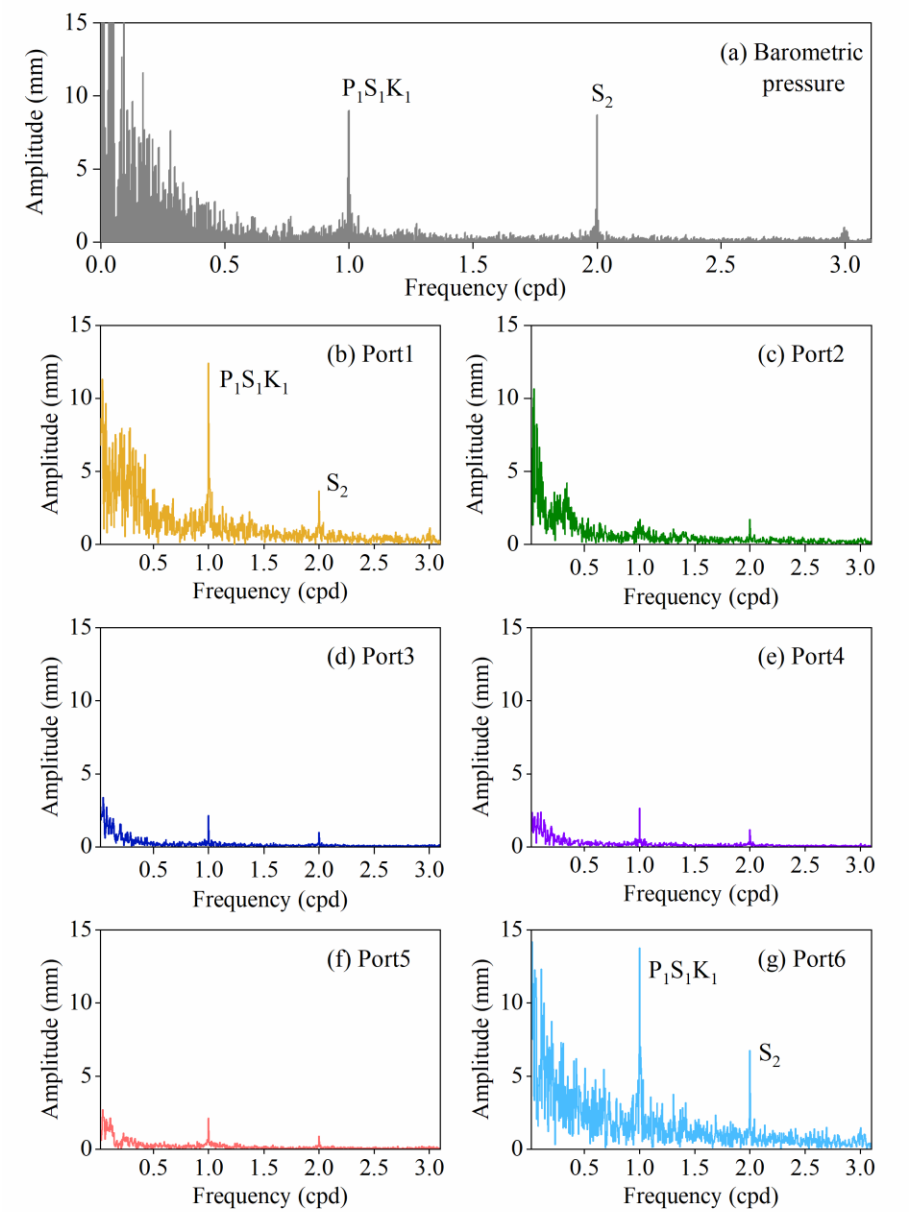

Figure 5. Amplitude spectra derived from FFT analysis: (a) barometric pressure, showing dominant diurnal (S_1) and semidiurnal (S_2) components; (b)–(g) groundwater level amplitude spectra for monitoring ports Port1 to Port6, respectively. Spectral peaks at ~1 and ~2 cpd reflect periodic atmospheric influences.

Table 1. Amplitudes of the main spectral components

Component	Frequency (cycles/day)	Origin	Barometric pressure (mm)	Port1 (mm)	Port2 (mm)	Port3 (mm)	Port4 (mm)	Port5 (mm)	Port6 (mm)

O_1	0.9295	Lunar diurnal	0.8352	0.9534	0.4967	0.1653	0.2066	0.2304	1.1941
P_1	0.9973	Solar diurnal	6.0704	7.5658	1.3227	0.9091	1.1581	1.3025	9.0848
S_1	1.0000	Solar diurnal	8.9761	12.3947	1.1406	2.1354	2.652	2.1456	13.6419
K_1	1.0027	Lunar-Solar diurnal	5.3492	7.195	1.5086	0.8417	1.1673	1.065	8.2521
N_2	1.8959	Lunar semi-diurnal	0.4721	0.7631	0.3831	0.1069	0.1187	0.0691	0.8009
M_2	1.9323	Lunar semi-diurnal	0.7387	0.3298	0.2572	0.1934	0.0766	0.0792	0.6084
S_2	2.0000	Solar semi-diurnal	8.6894	3.6595	1.7229	0.9772	1.1742	0.892	6.7347

3.4 Observed Barometric Response Functions

The frequency-domain barometric response of the well–aquifer system was quantified using barometric response functions (BRF), which characterize groundwater level fluctuations as a linear response to atmospheric pressure loading. In this framework, barometric pressure is treated as the input signal and groundwater level as the output, and the system behavior is described through a transfer function estimated in the frequency-domain (Bendat and Piersol, 1986; Quilty, 1991). The barometric pressure data were used in their original form (without filtering) to retain the full atmospheric pressure spectrum. The groundwater level time series, however, were high-pass filtered with a cutoff frequency of 0.02 cpd to remove low-frequency fluctuations related to recharge and long-term trends. This allowed for a more precise examination of the frequency-domain responses driven by barometric loading. The observed BRF in the frequency-domain is defined as:

$$BRF(\omega) = X_{WB}(\omega)/X_{BB}(\omega) \tag{3}$$

where $X_{WB}(\omega)$ denotes the cross-spectrum between groundwater level and barometric pressure, and $X_{BB}(\omega)$ is the auto-spectrum of barometric pressure, and ω is the angular frequency. The gain and phase response to the barometric pressure can be calculated by the modulus and the argument of $BRF(\omega)$, respectively:

$$G(\omega) = |BRF(\omega)| \tag{4}$$

$$\Phi(\omega) = \arg\{BRF(\omega)\} \tag{5}$$

While the BRF framework assumes linear system behavior, we recognize that the vadose zone can exhibit nonlinear responses due to the interactions between air and water in variably saturated conditions. The use of a linear framework in this study provides a simplified but practical means to quantify barometric pressure transmission. To quantify uncertainty in the estimated gain and phase, the normalized standard error $\sigma(\omega)$ was calculated to determine standard errors for gain, $\sigma A(\omega)$, and phase, $\sigma\theta(\omega)$ (Beavan et al., 1991; Bendat & Piersol, 2010; Hussein et al., 2013; Zhang et al., 2019b), which are given by:

$$\sigma(\omega) = \left[\frac{1}{2p}\left(\frac{1}{C_{xy}(\omega)^2}\right) - 1\right]^{1/2} \quad (6)$$

$$p = N - (N-1) \times \delta \quad (7)$$

$$\sigma A(\omega) = \sigma(\omega) \times gain(\omega),\ \sigma\theta(\omega) = \sigma(\omega) \times \frac{180}{\pi} \quad (8)$$

where $C_{xy}(\omega)$ is the coherence between the water level and barometric pressure, N is the number of segments, and δ is the percentage of overlap. The calculation of coherence and its role in defining the valid frequency range for BRF analysis are described in detail in Text S2.

In the present study, detailed BRF estimation was performed primarily for Ports 1 and 6. This selection was motivated by CCF and FFT analyses, which indicated that Ports 1 and 6 exhibited strong responses to atmospheric pressure variations throughout the monitoring period. In contrast, groundwater levels recorded at Ports 2-5 showed substantially attenuated barometric signals, with long response delays and spectral amplitudes close to background noise levels, which precluded reliable identification of barometric response functions. Port 1 is screened in the upper sandstone aquifer above the mudstone layer, whereas Port 6 is screened in the lower sandstone aquifer beneath the mudstone. These two monitoring intervals therefore represent

contrasting hydrostratigraphic conditions within the vertically layered system. Focusing on Ports 1 and 6 allows for a clear comparison of barometric response behavior above and below the low-permeability mudstone layer.

The transfer functions were estimated using Welch's averaged periodogram method (Welch, 1967), with a Hamming window applied to reduce spectral leakage (Lai et al., 2013). To capture more low-frequency information and ensure statistical stability across a broad frequency range, the same window–overlap combinations were applied consistently to both the groundwater level and barometric pressure data. Window lengths of 4320, 2880, and 1440 ten-minute intervals were used for both signals, with corresponding step sizes of 1440, 960, and 480 ten-minute intervals, respectively. These settings correspond to window durations of 30, 20, and 10 days at a 10-minute sampling interval, with approximately 66.7% overlap. Gain and phase frequency plots were generated to show estimates of barometric response functions for three overlapping frequency bands, with the number of segments N1, N2, and N3 corresponding to 233, 350, and 703.

The viable frequency range for BRF analysis was determined based on the frequency-dependent coherence between groundwater level and barometric pressure and spans 0.02–2 cpd (see Text S2 for details). This range encompasses the dominant diurnal and semidiurnal atmospheric pressure components while excluding low-frequency variability associated with recharge and long-term trends (Rojstaczer, 1988; Rojstaczer and Riley, 1990). Gain and phase estimates within this frequency band were combined across the three window configurations to obtain the final BRF. For consistency with the analytical solutions of Rojstaczer (1988), 180° was subtracted from the phase estimates. The resulting gain and phase spectra are shown in Figures 6a and 6b. Gain and phase values within the 0.02–2 cpd band were extracted to construct gain–

phase correlation plots (Figures 6c and 6d). Port 1 exhibits a negative gain–phase relationship, whereas Port 6 displays a positive gain–phase trend, indicating fundamentally different frequency-domain response behaviors at the two depths. These contrasting gain–phase patterns highlight systematic vertical differences in groundwater response to atmospheric loading within the layered aquifer system. The observed BRF provide the empirical basis for comparison with theoretical barometric response models, which are examined in the following section.

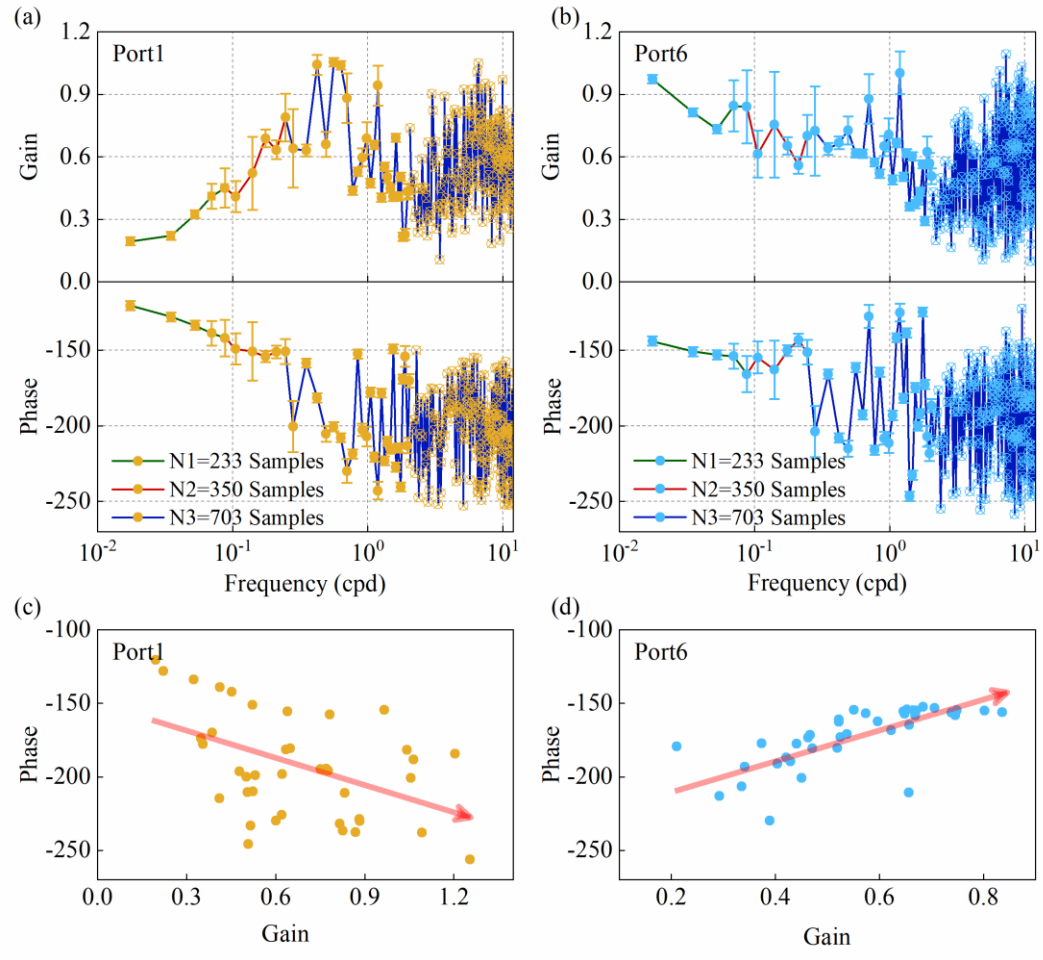

Figure 6. Observed barometric response function for Port 1 and Port 6: (a) Gain and phase spectra for Port 1, (b) Gain and phase spectra for Port 6, (c) Scatter plot of gain versus phase for Port 1 (0.02–2 cpd, showing a negative correlation), (d) Scatter plot of gain versus phase for Port 6 (0.02–2 cpd, showing a positive correlation).

3.5 Theoretical Barometric Response Functions

The frequency-domain barometric response model for a semi-confined aquifer incorporates three physically independent processes (Fig. 7a): (1) vertical air diffusion through the unsaturated zone; (2) vertical groundwater diffusion from the water table to the aquifer; and (3) horizontal groundwater flow between the aquifer and the wellbore. The theoretical BRF, expressed in terms of gain and phase, is given by:

$$Gain(\omega) = \left|\frac{x_0 \rho g}{A}\right| = \left|\frac{p_0 - A - s_0 \rho g}{A}\right| \tag{9}$$

$$Phase(\omega) = \arg\left(\frac{x_0 \rho g}{A}\right) = \arg\left(\frac{p_0 - A - s_0 \rho g}{A}\right) \tag{10}$$

where x_0 is the amplitude of water-level fluctuation in the well, A is the amplitude of barometric loading, ρ is water density, and g is gravitational acceleration. The terms p_0 and s_0 represent the aquifer pore-pressure response and the well drawdown response, respectively. These two terms are defined as:

$$p_0 = A(M + iN - 1 + BE) \cdot \exp[-(i+1) \cdot Q^{0.5}] + A \cdot (1 - BE) \tag{11}$$

$$s_0 = i0.5 W x_0 K_0 \left\{\left[W^2 \left[{S_{aqu}}^2 + \left(\frac{S_{con}}{2Q}\right)^2\right]\right]^{0.25} \cdot exp\left[0.5 \tan^{-1}\left[2Q \cdot \frac{S_{aqu}}{S_{con}}\right]\right]\right\} \tag{12}$$

where BE is the static barometric efficiency. The coefficients M and N describe the pneumatic response of the unsaturated zone and are given by:

$$M = \frac{2\cosh(\sqrt{R})\cos(\sqrt{R})}{\cosh(2\sqrt{R}) + \cos(2\sqrt{R})},\ N = \frac{2\sinh(\sqrt{R})\sin(\sqrt{R})}{\cosh(2\sqrt{R}) + \cos(2\sqrt{R})} \tag{13}$$

where K_0 is the modified Bessel function of the second kind and order zero, and S_{aqu} and S_{con} denote the storativity of the aquifer and confining layer, respectively. The dimensionless

parameters R, Q, and W describe the frequency-dependent behavior of the three governing processes and are defined as:

$$R = \frac{{L_{unsat}}^2 \omega}{2D_{unsat}},\ Q = \frac{{L_{con}}^2 \omega}{2D_{con}},\ W = \frac{{r_w}^2 \omega}{T_{aqu}} \tag{14}$$

where L_{unsat} and D_{unsat} are the thickness and pneumatic diffusivity of the unsaturated zone, L_{con} and D_{con} are the thickness and hydraulic diffusivity of the confining layer, r_w is the well radius, and T_{aqu} is the aquifer transmissivity.

Figure 7b shows theoretical BRF of the semi-confined aquifer model was computed to simulate groundwater responses (BE = 0.5). R is assumed to be much less than Q (R/Q = 0.0001), with specific storage parameters S_{con} and S_{aqu} are set to 10^{-4}. The dimensionless parameter Q/W was varied from 10^{-1}~10^{3}. In the low-frequency range, the well is assumed to be in pressure equilibrium with the aquifer (i.e., s_0=0), where barometric loading is modulated primarily by air diffusion in the unsaturated zone and vertical groundwater diffusion. This configuration is representative of wells in unconfined or weakly confined settings, where overlying materials dominate pressure transmission. In this case, the model simplifies to the following equation for gain:

$$Gain(\omega) = \left|\frac{p_0}{A} - 1\right| \tag{15}$$

In the high-frequency range, the aquifer responds more rapidly than the well, and the effects of the unsaturated zone and confining layer become negligible. Here, the aquifer pore pressure can be considered effectively constant ($Q \rightarrow \infty$), and groundwater response is governed mainly by well-aquifer interactions. This scenario applies to wells in confined aquifers, where barometric loading propagates directly into the aquifer with minimal attenuation from overlying layers. The model is reduced to:

$$Gain(\omega) = \left| \frac{S_0 \rho g}{A} + BE \right| \quad (16)$$

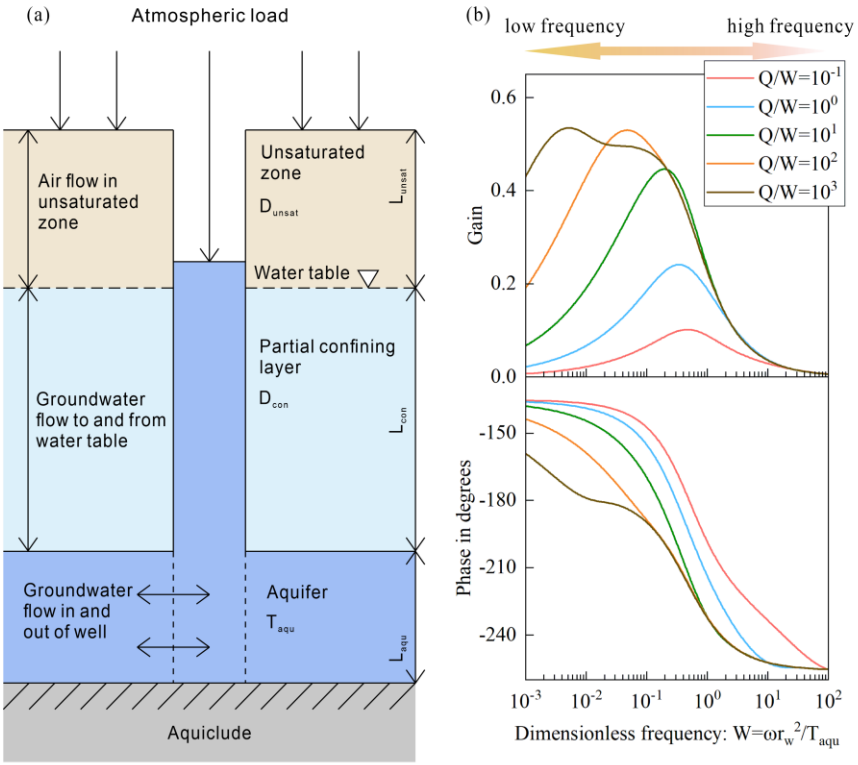

Figure 7. (a) Idealized representation of open wells under barometric loading in a semi-confined aquifer, incorporating air diffusion, vertical groundwater flow, and well-aquifer interaction (modified from Rojstaczer, 1988); (b) Theoretical BRF for semi-confined aquifers with fixed R/Q, S_{con}, and S_{aqu} but varying Q/W.

These two end-member cases of the semi-confined model, representing unconfined (Fig. 8a) and confined aquifer (Fig. 8b) behavior, then theoretical BRFs were computed under different contrasting aquifer conditions (BE = 0.5).The dimensionless parameter R/Q was set from 10^{-1}~10^{3} in the unconfined aquifer model (Fig. 8c), while for the confined aquifer model (Fig. 8d), aquifer storativity S_{aqu} ranged from 10^{-7}~10^{-3}. Figures 8e and 8f show gain–phase data points from different frequency bands, a selection that ensures each aquifer model is evaluated within the frequency domain where its characteristic response mechanisms dominate. In the unconfined

model, the gain–phase curves were analyzed over the low-frequency range of 10^{-3}~0.5 cpd, which is below the characteristic transition frequency associated with pressure diffusion through the unsaturated zone and overlying materials. The result shows that unconfined systems exhibit a negative correlation between gain and phase. However, for large values of R/Q, a transition from negative to positive correlation occurs at higher frequencies, reflecting a shift from diffusion-dominated to elasticity-dominated behavior. The characteristic transition frequency thus shifts towards lower frequencies (Bendat & Piersol, 2010). In contrast, the confined model was evaluated within a higher frequency range of 0.02~2 cpd, encompassing diurnal and semi-diurnal barometric components, where pressure transmission is dominated by aquifer–well elastic interaction, resulting in a pronounced positive gain–phase correlation.

As demonstrated in Figure 6, Port 1 exhibits a negative gain–phase correlation, consistent with unconfined behavior, while Port 6 shows a positive gain–phase trend, indicative of confined behavior. These contrasting patterns highlight fundamental differences in vertical hydraulic connectivity and pressure transmission mechanisms.

Theoretical BRF models are used here not for parameter inversion but to provide a reference framework for interpreting observed frequency-domain responses. Due to the strong parameter coupling and non-uniqueness inherent in semi-confined models, direct fitting of model parameters with barometric data alone is not feasible without independent constraints. Thus, we adopt a response-based comparison approach, focusing on the qualitative and semi-quantitative correspondence between observed gain–phase trends and theoretical end-member behaviors.

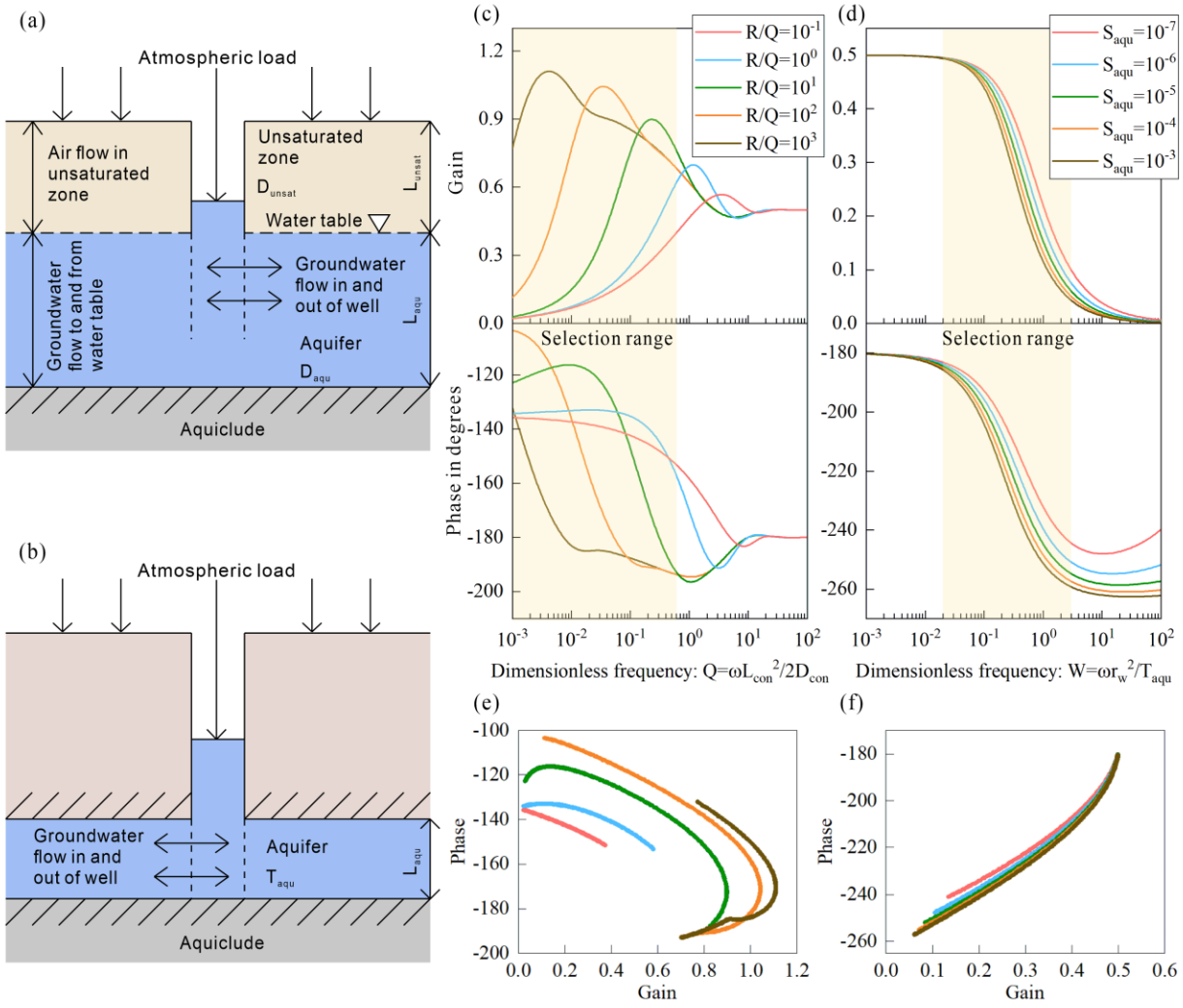

Fig. 8. (a) Conceptual model of an unconfined aquifer governed by unsaturated and confining layer diffusion (modified from Rojstaczer, 1988); (b) Conceptual model of a confined aquifer dominated by well-aquifer interaction (modified from Rojstaczer, 1988); (c) Theoretical BRF for unconfined aquifers with varying R/Q and Q; (d) Theoretical BRF for confined aquifers with varying Saqu, represented through variations in W (BE = 0.5); (e) Gain–phase data points for selected frequencies in the unconfined model; (f) Gain–phase data points for selected frequencies in the confined model.

4 Discussion

Groundwater responses to barometric pressure, particularly within vertically distributed monitoring systems, provide valuable insights into aquifer confinement and pressure transmission mechanisms. Time-domain cross-correlation and frequency-domain spectral analyses across six monitoring ports consistently revealed pronounced contrasts in barometric response behavior between sandstone and mudstone intervals. All ports exhibited inverse barometric responses, with systematic variations in response lags and spectral amplitudes according to lithology. These results suggest that hydrostratigraphic contrasts, rather than monitoring depth alone, exert a dominant influence on pressure transmission dynamics. Ports screened within sandstone units exhibited shorter response lags and higher spectral amplitudes, whereas those located within or adjacent to mudstone layers displayed attenuated and delayed responses, highlighting the strong damping effect imposed by low-permeability strata.

FFT analyses further demonstrated that atmospheric pressure signals at diurnal and semi-diurnal frequencies were consistently recorded in groundwater level spectra, with higher amplitudes in sandstone-associated ports compared to mudstone-associated intervals. This indicates that vertical heterogeneity in barometric pressure transmission is primarily governed by hydrostratigraphic contrasts, with even relatively thin mudstone layers significantly attenuating and delaying pressure signals. These findings provide the foundation for interpreting contrasting gain–phase relationships observed in frequency-domain BRF analyses.

In semi-confined aquifers, the barometric response function exhibits a pronounced frequency dependence, which can be divided into three distinct bands. The low-frequency response is controlled by vertical pneumatic diffusivity and thickness of the unsaturated zone, and by vertical hydraulic diffusivity and thickness of the confining unit. The mid-frequency response

corresponds to static barometric efficiency, while the high-frequency response is increasingly influenced by well–aquifer interaction. The unconfined aquifer system exhibits similar frequency-dependent behavior, also dividing into three bands. At low frequencies, the response is largely governed by the aquifer's specific yield, storativity, and vertical hydraulic conductivity. Mid-frequency behavior reflects the relative magnitudes of gas diffusivity in the unsaturated zone and vertical hydraulic diffusivity within the aquifer. At high frequencies, a phase plateau near –180° emerges, with the unsaturated zone functioning similarly to a confining layer, resulting in gain magnitudes comparable to the static barometric efficiency expected under confined conditions. Port 1, screened in an upper sandstone unit, reflects typical free-surface conditions consistent with an unconfined aquifer. Spectrally, Port 1 exhibits an inverse trend between gain and phase across low- to mid-frequency ranges, where gain slightly increases while phase decreases with frequency. This negative gain-phase correlation is typical of unconfined systems, influenced by vadose zone thickness, air–water interactions, and boundary heterogeneity (Rojstaczer & Riley, 1990; Li et al., 2012). Although similar patterns can appear in semi-confined systems over specific frequency bands, Port 1's geological context and static water table conditions suggest it most closely represents a typical unconfined aquifer response.

In confined aquifer systems, barometric disturbances propagate rapidly via elastic deformation of both pore water and the aquifer matrix, leading to coherent and prompt water level responses, particularly at low frequencies. Gain decreases monotonically with frequency, and phase lag progressively shifts, resulting in a persistent positive correlation between gain and phase. This synchronized decay reflects the elastic storage response, primarily governed by aquifer-specific storativity (S_o) (Narasimhan & Kanehiro, 1984; Rojstaczer, 1988). Port 6, screened in the lower sandstone aquifer beneath a thin mudstone layer, exhibits a positive gain-phase relationship

typical of a confined system, reflecting functional confinement induced by the low-permeability mudstone layer. While confined-like responses were observed at Port 6, these are more likely attributable to localized hydraulic impedance imposed by the thin mudstone layer, rather than indicating a fully confined aquifer in the traditional sense. This highlights the scale sensitivity of BRF analysis, emphasizing its ability to detect functional confinement even in systems with fine vertical resolution.

The joint evolution of gain and phase across frequencies provides a robust framework for interpreting barometric response behavior in vertically heterogeneous groundwater systems. Rather than serving as a strict classification tool, gain-phase co-variation reflects frequency-dependent response regimes influenced by pressure transmission pathways, storage mechanisms, and hydraulic impedance imposed by low-permeability layers. Monitoring intervals exhibiting opposite or synchronous gain-phase trends correspond to contrasting modes of barometric signal propagation, closely related to differences in functional confinement and vertical hydraulic connectivity. This response-based approach transcends static lithologic descriptions, offering a dynamic interpretation of aquifer behavior under atmospheric forcing.

It is important to note that the high-pass filtering used to remove rainfall effects inherently suppresses low-frequency groundwater dynamics related to long-term recharge or storage processes. Although zero-phase filtering was applied to avoid phase distortion, the magnitude of phase lag is sensitive to preprocessing choices. As such, phase-based interpretations in this study are emphasized comparatively rather than as absolute metrics, focusing on relative differences in barometric response characteristics.

5 Conclusions

This study investigated groundwater responses to barometric loading using a vertically distributed multilevel monitoring system in a layered aquifer. Time-domain cross-correlation and frequency-domain spectral analyses across six monitoring ports revealed pronounced lithology-controlled differences in groundwater responses to atmospheric pressure variations. Monitoring ports screened within sandstone units exhibited stronger barometric signals, whereas those located within or adjacent to mudstone layers showed markedly attenuated responses, highlighting the damping effect imposed by low-permeability strata on pressure transmission.

Frequency-domain barometric response function (BRF) analysis conducted for the two most barometrically sensitive ports further highlighted contrasting response behaviors. Port 1 located in the upper unconfined sandstone exhibited a negative gain–phase co-variation, consistent with delayed and attenuated pressure transmission influenced by unsaturated zone buffering and drainage processes. In contrast, Port 6 screened in sandstone beneath a thin mudstone layer displayed a positive gain–phase relationship, indicative of a confined-like elastic response characterized by synchronous attenuation of gain and phase. Comparison with theoretical BRF models demonstrates that these contrasting gain–phase patterns arise from fundamentally different pressure transmission regimes associated with unconfined and functionally confined conditions. This study specifically emphasized functional confinement, which reflects pressure transmission controlled by the elastic properties of the aquifer and overlying materials, as opposed to the traditional rigid-flow assumption that treats confinement as a static condition governed by impermeable layers.

Overall, the results show that vertically resolved, frequency-domain analysis of barometric responses provides a robust, physically grounded framework for interpreting pressure transmission

behavior and vertical hydraulic connectivity in heterogeneous aquifer systems. Rather than serving as a strict classification tool for aquifer types, gain–phase co-variation reflects frequency-dependent response regimes controlled by hydrostratigraphic structure and hydraulic impedance. This response-based perspective underscores the value of multilevel groundwater monitoring under natural atmospheric forcing for elucidating subsurface pressure dynamics in layered systems. The study demonstrates the potential of frequency-domain BRF analysis for quantifying vertical heterogeneity in pressure transmission mechanisms in layered aquifer systems. It highlights the utility of this approach in interpreting functional confinement and vertical hydraulic connectivity based on observed barometric response behaviors.

Acknowledgments

This research is financially supported by the Opening Fund of State Key Laboratory of Geohazard Prevention and Geoenvironment Protection (SKLGP2017K001 and SKLGP2018K003), and Program of China Scholarship Council (Grant No.202409230004).

Open Research

Data are available upon reasonable request from the corresponding author.

References

Acworth, R. I., Rau, G. C., Halloran, L. J., & Timms, W. A. (2017). Vertical groundwater storage properties and changes in confinement determined using hydraulic head response to atmospheric tides. Water Resources Research, 53(4), 2983-2997. https://doi.org/10.1002/2016WR020311

Akara, M. E. M., Kuhlman, K. L., Bowman Ii, D. O., & Jackson, R. S. (2025). Factors controlling groundwater response to earth and atmospheric tides. Journal of Hydrology, 657, 133088. https://doi.org/10.1016/j.jhydrol.2025.133088

571 Barco, J., Hogue, T. S., Girotto, M., Kendall, D. R., & Putti, M. (2010). Climate signal
572 propagation in southern California aquifers. Water resources research, 46(10).
573 https://doi.org/10.1029/2009WR008376

574 Bendat, J. S., & Piersol, A. G. (2011). Random data: analysis and measurement procedures. John
575 Wiley & Sons.

576 Bui, D. D., Kawamura, A., Tong, T. N., Amaguchi, H., & Trinh, T. M. (2012). Aquifer system
577 for potential groundwater resources in Hanoi, Vietnam. Hydrological Processes, 26(6), 932-946.
578 https://doi.org/10.1002/hyp.8305

579 Butler Jr, J. J., Jin, W., Mohammed, G. A., & Reboulet, E. C. (2011). New insights from well
580 responses to fluctuations in barometric pressure. Groundwater, 49(4), 525-533.
581 https://doi.org/10.1111/j.1745-6584.2010.00768.x

582 Chapman, S., & Lindzen, R. S. (1969). Atmospheric tides: thermal and gravitational (Vol. 15).
583 Springer Science & Business Media.

584 Davis, J. C., & Sampson, R. J. (1986). Statistics and data analysis in geology (Vol. 646). New
585 York: Wiley.

586 Elkhoury, J. E., Brodsky, E. E., & Agnew, D. C. (2006). Seismic waves increase permeability.
587 Nature, 441(7097), 1135-1138. https://doi.org/10.1038/nature04798

588 Evans, K., Beavan, J., Simpson, D., & Mousa, S. (1991). Estimating aquifer parameters from
589 analysis of forced fluctuations in well level: An example from the Nubian Formation near
590 Aswan, Egypt: 3. Diffusivity estimates for saturated and unsaturated zones. Journal of
591 Geophysical Research: Solid Earth, 96(B7), 12161-12191. https://doi.org/10.1029/91jb00957

592 Furbish, D. J. (1991). The response of water level in a well to a time series of atmospheric
593 loading under confined conditions. Water Resources Research, 27(4), 557-568.
594 https://doi.org/10.1029/90WR02775

595 Gulley, J., Martin, J., Spellman, P., Moore, P., & Screaton, E. (2013). Dissolution in a variably
596 confined carbonate platform: effects of allogenic runoff, hydraulic damming of groundwater
597 inputs, and surface–groundwater exchange at the basin scale. Earth Surface Processes and
598 Landforms, 38(14), 1700-1713. https://doi.org/10.1002/esp.3411

599 Hussein, M. E., Odling, N. E., & Clark, R. A. (2013). Borehole water level response to
600 barometric pressure as an indicator of aquifer vulnerability. Water Resources Research, 49(10),
601 7102-7119. https://doi.org/10.1002/2013WR014134

602 Jacob, C. E. (1940). On the flow of water in an elastic artesian aquifer. Transactions American
603 Geophysical Union, 21(2), 574-586. https://doi.org/10.1029/TR021i002p00574

604 Jan, C. D., Chen, T. H., & Lo, W. C. (2007). Effect of rainfall intensity and distribution on
605 groundwater level fluctuations. Journal of hydrology, 332(3-4), 348-360.
606 https://doi.org/10.1016/j.jhydrol.2006.07.010

607 Kennel, J., & Parker, B. (2024). Characterizing water level responses to barometric pressure
608 fluctuations from seconds to days. Journal of Hydrology, 641, 131843.
609 https://doi.org/10.1016/j.jhydrol.2024.131843

610 Koh, E. H., Lee, E., & Lee, K. K. (2016). Impact of leaky wells on nitrate cross-contamination in
611 a layered aquifer system: Methodology for and demonstration of quantitative assessment and
612 prediction. Journal of Hydrology, 541, 1133-1144. https://doi.org/10.1016/j.jhydrol.2016.08.019

613 Lai, G. J., Ge, H. K., & Wang, W. L. (2013). Transfer functions of the well-aquifer systems
614 response to atmospheric loading and Earth tide from low to high-frequency band. Journal of
615 Geophysical Research: Solid Earth, 118 (5), 1904-1924. https://doi.org/10.1002/jgrb.50165

616 Landmeyer, J. E. (1996). Aquifer response to record low barometric pressures in the southeastern
617 United States. Groundwater, 34(5), 917-924. https://doi.org/10.1111/j.1745-6584.1996.tb02086.x

618 Li, J., You, K., Zhan, H., & Huang, G. (2012). Analytical solution to subsurface air pressure in a
619 three-layer unsaturated zone with atmospheric pressure changes. Transport in porous media,
620 93(3), 461-474. https://doi.org/ 10.1007/s11242-012-9964-5

621 Liu, W., Du, Y., Qiu, W., Deng, Y., & Wang, Y. (2025). Constraints on vertical variability of
622 geogenic ammonium in multi-layered aquifer systems. Water Research, 268, 122639.
623 https://doi.org/10.1016/j.watres.2024.122639

624 Luo, H., Li, Z., Luo, M., Zhang, Q., & Illman, W. A. (2020). An analytical method to calculate
625 groundwater released from an aquitard undergoing nonlinear consolidation. Water Resources
626 Research, 56(9), e2020WR027320. https://doi.org/10.1029/2020WR027320

627 Maliva, R. G., & Walker, C. W. (1998). Hydrogeology of deep-well disposal of liquid wastes in
628 southwestern Florida, USA. Hydrogeology Journal, 6(4), 538-548.
629 https://doi.org/10.1007/s100400050174

630 Manna, F., Kennel, J., & Parker, B. L. (2022). Understanding mechanisms of recharge through
631 fractured sandstone using high-frequency water-level-response data. Hydrogeology Journal,
632 30(5), 1599-1618. https://doi.org/10.1007/s10040-022-02515-3

McMillan, T. C., Rau, G. C., Timms, W. A., & Andersen, M. S. (2019). Utilizing the impact of Earth and atmospheric tides on groundwater systems: A review reveals the future potential. Reviews of Geophysics, 57(2), 281-315. https://doi.org/10.1029/2018RG000630

Merritt, M. L. (2004). Estimating hydraulic properties of the Floridan aquifer system by analysis of earth-tide, ocean-tide, and barometric effects, Collier and Hendry Counties, Florida (No. 3). US Department of the Interior, US Geological Survey.

Molenat, J., Davy, P., Gascuel-Odoux, C., & Durand, P. (1999). Study of three subsurface hydrologic systems based on spectral and cross-spectral analysis of time series. Journal of Hydrology, 222(1-4), 152-164. https://doi.org/10.1016/S0022-1694(99)00107-9

Narasimhan, T. N., Kanehiro, B. Y., & Witherspoon, P. A. (1984). Interpretation of earth tide response of three deep, confined aquifers. Journal of Geophysical Research: Solid Earth, 89(B3), 1913-1924. https://doi.org/10.1029/JB089iB03p01913

Odling, N. E., Serrano, R. P., Hussein, M. E. A., Riva, M., & Guadagnini, A. (2015). Detecting the vulnerability of groundwater in semi-confined aquifers using barometric response functions. Journal of Hydrology, 520, 143-156. https://doi.org/10.1016/j.jhydrol.2014.11.016

Padilla, A., & Pulido-Bosch, A. (1995). Study of hydrographs of karstic aquifers by means of correlation and cross-spectral analysis. Journal of hydrology, 168(1-4), 73-89. https://doi.org/10.1016/0022-1694(94)02648-U

Patton, A. M., Rau, G. C., Cleall, P. J., & Cuthbert, M. O. (2021). Hydro-geomechanical characterisation of a coastal urban aquifer using multiscalar time and frequency domain groundwater-level responses. Hydrogeology Journal, 29(8), 2751-2771. https://doi.org/10.1007/s10040-021-02400-5

Qi, Z., Shi, Z., & Rasmussen, T. C. (2023). Time-and frequency-domain determination of aquifer hydraulic properties using water-level responses to natural perturbations: A case study of the Rongchang Well, Chongqing, southwestern China. Journal of Hydrology, 617, 128820. https://doi.org/10.1016/j.jhydrol.2022.128820

Qi, Z., Shi, Z., Rasmussen, T., Guo, H., & Wang, G. (2024). Investigating the Representative of Aquifer Transmissivity Determined by Passive Response Methods: A Comparison With Time-Dependent Hydraulic Parameters Inferred From Different Stages of Pumping Tests. Water Resources Research, 60(2), e2022WR033952. https://doi.org/10.1029/2022WR033952

Qin, Z., Guo, J., Maldaner, C. H., Bairos, K., Xu, Q., Cherry, J. A., & Parker, B. L. (2025). Using barometric response functions to estimate unconfined aquifer permeability changes caused by landslide: A case study in southwest China. Engineering Geology, 348, 107950. https://doi.org/10.1016/j.enggeo.2025.107950

Quilty, E. G., & Roeloffs, E. A. (1991). Removal of barometric pressure response from water level data. Journal of Geophysical Research, 96(B6), 10209-10218. https://doi.org/10.1029/91JB00429

Rasmussen, T.C., & Crawford, L.A. (1997). Identifying and removing barometric pressure effects in confined and unconfined aquifers. Groundwater, 35 (3), 502–511. https://doi.org/10.1111/j.1745-6584.1997.tb00111.x

Rausch, R., & Dirks, H. (2024). A hydrogeological overview of the Upper Mega Aquifer System on the Arabian Platform. Hydrogeology Journal, 32(2), 621-634. https://doi.org/10.1007/s10040-023-02760-0

676 Rojstaczer, S. (1988). Determination of fluid flow properties from the response of water levels in
677 wells to atmospheric loading. Water Resources Research, 24(11), 1927-1938.
678 https://doi.org/10.1029/WR024i011p01927

679 Rojstaczer, S., & Agnew, D. C. (1989). The influence of formation material properties on the
680 response of water levels in wells to Earth tides and atmospheric loading. Journal of Geophysical
681 Research: Solid Earth, 94(B9), 12403-12411. https://doi.org/10.1029/JB094iB09p12403

682 Rojstaczer, S., & Riley, F. S. (1990). Response of the water level in a well to Earth tides and
683 atmospheric loading under unconfined conditions. Water Resources Research, 26(8), 1803-1817.
684 https://doi.org/10.1029/WR026i008p01803

685 Shi, L., Zhang, B., Wang, L., Wang, H. X., & Zhang, H. J. (2018). Functional efficiency
686 assessment of the water curtain system in an underground water-sealed oil storage cavern based
687 on time-series monitoring data. Engineering Geology, 239, 79-95.
688 https://doi.org/10.1016/j.enggeo.2018.03.015

689 Spane, F. A. (2002). Considering barometric pressure in groundwater flow investigations. Water
690 resources research, 38(6), 14-1. https://doi.org/10.1029/2001WR000701

691 Sun, X., & Xiang, Y. (2019). Heterogeneous permeability changes along a fault zone caused by
692 the Xingwen M5. 7 earthquake in SW China. Geophysical Research Letters, 46(24), 14404-
693 14411. https://doi.org/10.1029/2019GL085673

694 Sun, X., & Xiang, Y. (2020). Comparison of transfer function models for well-aquifer system
695 response to atmospheric loading. Journal of Hydrology, 590, 125494.
696 https://doi.org/10.1016/j.jhydrol.2020.125494

Thomas, A., Fortin, J., Vittecoq, B., & Violette, S. (2023). Earthquakes and heavy rainfall influence on aquifer properties: A new coupled Earth and barometric tidal response model in a confined bi-layer aquifer. Water Resources Research, 59(4), e2022WR033367. https://doi.org/10.1029/2022WR033367

Valois, R., Derode, B., Vouillamoz, J. M., Valerie Kotchoni, D. O., Lawson, M. A., & Rau, G. C. (2023). Use of atmospheric tides to estimate the hydraulic conductivity of confined and semi-confined aquifers. Hydrogeology Journal, 31(8), 2115-2128. https://doi.org/10.1007/s10040-023-02715-5

Wang, C. Y., & Manga, M. (2023). Changes in tidal and barometric response of groundwater during earthquakes—A review with recommendations for better management of groundwater resources. Water, 15(7), 1327. https://doi.org/10.3390/w15071327

Wang, G., Liang, X., Li, J., Wang, J., & Wang, C. Y. (2024). Impact of depth-dependent heterogeneity in aquifers on the response of unsaturated-saturated flow to Earth tides. Water Resources Research, 60(6), e2023WR036310. https://doi.org/10.1029/2023WR036310

Weeks, E.P. (1979). Barometric fluctuations in wells tapping deep unconfined aquifers. Water Resources Research, 15(5), 1167-1176. https://doi.org/10.1029/WR015i005p01167

Welch, P. D. (1967), The use of fast Fourier transform for the estimation of power spectra: A method based on time averaging over short, modified periodograms, IEEE Trans. Audio Electroacoust., 15(2), 70–73. https://doi.org/10.1109/TAU.1967.1161901.

Xu, Q., Li, W. H., Liu, H. X., Tang, R., Chen, S. J., & Sun, X. (2015). Hysteresis effect on the deep-Seated landslide by rainfall: The case of the Kualiangzi landslide, China. Paper presented at IAEG XII Congress, Torino, Italy.

719 Yang, M., Annable, M. D., & Jawitz, J. W. (2017). Forward and back diffusion through
720 argillaceous formations[J]. Water Resources Research, 53(5), 4514-4523.
721 https://doi.org/10.1002/2016WR019874
722 Zhang, H., Shi, Z., Wang, G., Sun, X., Yan, R., & Liu, C. (2019). Large earthquake reshapes the
723 groundwater flow system: Insight from the water- level response to earth tides and atmospheric
724 pressure in a deep well. Water Resources Research, 55(5), 4207-4219.
725 https://doi.org/10.1029/2018WR024608